

Phase Retrieval Using Feasible Point Pursuit: Algorithms and Cramér-Rao Bound

Cheng Qian, *Student Member, IEEE*, Nicholas D. Sidiropoulos, *Fellow, IEEE*, Kejun Huang, *Student Member, IEEE*, Lei Huang, *Senior Member, IEEE* and H. C. So, *Fellow, IEEE*

Abstract—Reconstructing a signal from squared linear (rank-one quadratic) measurements is a challenging problem with important applications in optics and imaging, where it is known as *phase retrieval*. This paper proposes two new phase retrieval algorithms based on non-convex quadratically constrained quadratic programming (QCQP) formulations, and a recently proposed approximation technique dubbed *feasible point pursuit (FPP)*. The first is designed for uniformly distributed bounded measurement errors, such as those arising from high-rate quantization (B-FPP). The second is designed for Gaussian measurement errors, using a least squares criterion (LS-FPP). Their performance is measured against state-of-the-art algorithms and the Cramér-Rao bound (CRB), which is also derived here. Simulations show that LS-FPP outperforms the state-of-the-art and operates close to the CRB. Compact CRB expressions, properties, and insights are obtained by explicitly computing the CRB in various special cases – including when the signal of interest admits a sparse parametrization, using harmonic retrieval as an example.

Index Terms—Phase retrieval, quadratically constrained quadratic programming (QCQP), semidefinite programming (SDP), feasible point pursuit (FPP), Cramér-Rao bound (CRB).

I. INTRODUCTION

Phase retrieval (PR) is the problem of reconstructing a signal $\mathbf{x} \in \mathbb{C}^N$ from measurements of the form

$$y_i = |\mathbf{a}_i^H \mathbf{x}|^2, \quad i \in \{1, \dots, M\} \quad (1)$$

where $|\cdot|$ is the magnitude of a complex number, $(\cdot)^H$ is the conjugate transpose and $\mathbf{a}_i \in \mathbb{C}^N$ is a known measurement vector. The above problem appears in many applications such as crystallography [1], diffraction imaging [2]-[3] and microscopy [4]-[5], where it is often far easier to measure the magnitude than the phase.

During the past decades, numerous phase retrieval solvers have been developed in the literature. Among them, the Gerchberg-Saxton [6] and Fienup [7] algorithms are the most well-known and widely used methods in practice. These approaches are based on alternating optimization in which the

Original manuscript submitted to *IEEE Trans. on Signal Processing*, November 28, 2018. C. Qian, N. D. Sidiropoulos and K. Huang are with the Department of Electrical and Computer Engineering, University of Minnesota, Minneapolis, MN 55455 USA (e-mail: qianc@umn.edu, nikos@umn.edu, huang663@umn.edu). L. Huang is with the College of Information Engineering, Shenzhen University, Shenzhen, 518060 China (e-mail: dr.lei.huang@ieee.org). H. C. So is with the Department of Electronic Engineering, City University of Hong Kong, Hong Kong, China (e-mail: hcso@ee.cityu.edu.hk). The work of N. Sidiropoulos was supported by NSF CIF-1525194. K. Huang was supported by a UMII dissertation fellowship. C. Qian is on leave from the Department of Electronics and Information Engineering, Harbin Institute of Technology, China, supported in part by the Natural Science Foundation of China (NSFC) under Grant No. 61171187 and the Chinese Scholarship Council.

unknown \mathbf{x} is iteratively estimated by solving a least squares (LS) problem, i.e.,

$$\min_{\mathbf{x}, \mathbf{u} \mid |u_i|=1, \forall i} \|\sqrt{\mathbf{y}} \odot \mathbf{u} - \mathbf{A}^H \mathbf{x}\|_2^2 \quad (2)$$

where $\mathbf{y} = [y_1 \dots y_M]^T$ is the data vector, $\mathbf{A} = [\mathbf{a}_1 \dots \mathbf{a}_M]$ is the known measurement matrix, \mathbf{u} is the phase of $\sqrt{\mathbf{y}}$ (an extra unknown, together with \mathbf{x}), $\|\cdot\|_2$ is the 2-norm and $\odot \cdot$ denotes element-wise multiplication. The main problem with this type of algorithms is that they tend to hit local minima, thus requiring careful initialization, and often fail to perform satisfactorily even after multiple initializations.

Recently, modern convex relaxation techniques were applied to phase retrieval. *PhaseLift* [8]-[9] employs matrix lifting to recast phase retrieval as a semi-definite programming (SDP) problem. Specifically, the PhaseLift scheme regards the measurements in (1) as a linear function of $\mathbf{X} = \mathbf{x}\mathbf{x}^H$ which is a rank-1 Hermitian matrix, i.e.,

$$y_i = |\mathbf{a}_i^H \mathbf{x}|^2 = \mathbf{x}^H \mathbf{a}_i \mathbf{a}_i^H \mathbf{x} = \text{tr}(\mathbf{A}_i \mathbf{X}) \quad (3)$$

where $\mathbf{A}_i = \mathbf{a}_i \mathbf{a}_i^H$ and $\text{tr}(\cdot)$ denotes the trace of a matrix. Thus, the recovery of \mathbf{x} is equivalent to finding a positive semidefinite rank-1 matrix \mathbf{X} ($\mathbf{X} \succeq 0$) through solving a rank minimization problem:

$$\begin{aligned} \min_{\mathbf{X}} \text{rank}(\mathbf{X}) \\ \text{s.t. } y_i = \text{tr}(\mathbf{A}_i \mathbf{X}), \quad i \in \{1, \dots, M\} \\ \mathbf{X} \succeq 0. \end{aligned} \quad (4)$$

Since rank minimization is a non-convex problem which is difficult to solve in a computationally efficient manner, PhaseLift relaxes the problem in (4) via semidefinite relaxation – see [10] for a tutorial overview. It has been shown in [8] that if the measurement vectors are i.i.d. Gaussian distributed, then PhaseLift can recover \mathbf{x} with high probability when the number of measurements $M \sim \mathcal{O}(N \log N)$. However, when the measurements are corrupted by noise, there is no guarantee that PhaseLift will yield a rank-1 solution [11].

PhaseCut [12] takes a similar approach as PhaseLift, but instead of directly aiming for \mathbf{x} it tries to find \mathbf{u} first. Substituting the conditional LS estimate¹ $\hat{\mathbf{x}} = (\mathbf{A}^H)^\dagger \text{diag}(\sqrt{\mathbf{y}})\mathbf{u}$ of \mathbf{x} given \mathbf{u} , PhaseCut aims at recovering \mathbf{u} by solving the non-convex quadratic program

$$\begin{aligned} \min_{\mathbf{u}} \mathbf{u}^H \mathbf{M} \mathbf{u} \\ \text{s.t. } |u_i| = 1, \quad i \in \{1, \dots, M\} \end{aligned} \quad (5)$$

¹ $(\cdot)^\dagger$ denotes the pseudo-inverse.

where $\mathbf{M} = \text{diag}(\sqrt{y})(\mathbf{I}_M - \mathbf{A}^H(\mathbf{A}^H)^\dagger)\text{diag}(\sqrt{y})$ with \mathbf{I}_M being a $M \times M$ identity matrix. Formulation (5) resembles the classical *MaxCut* problem in networks, enabling fast semidefinite relaxation algorithms originally developed for *MaxCut* to be adapted for *PhaseCut*. This makes *PhaseCut* faster than *PhaseLift*.

More recently, a new approach to phase retrieval was proposed, in what appears to be an instance of a new algorithmic genre that relies on smart ‘statistical’ initialization followed by relatively simple descent-type refinement named *Wirtinger Flow (WF)* [13]. It has been theoretically shown that when sufficiently many i.i.d. Gaussian measurement vectors are used, WF will recover the desired solution with high probability. However, recovery cannot be guaranteed when the number of measurements is small, or when the measurement vectors are not random – mainly because the principal eigenvector used for initialization is not a good approximation of \mathbf{x} in such cases. This means that for systematic (non-random) measurement designs and/or relatively short sample sizes there is considerable room for improvement.

In this paper, the focus is on recovering \mathbf{x} from noisy measurements, i.e.,

$$y_i = |\mathbf{a}_i^H \mathbf{x}|^2 + n_i, \quad i \in \{1, \dots, M\} \quad (6)$$

where n_i is additive noise. To this end, in Section II, two novel algorithms are developed. These algorithms build upon a method called *feasible point pursuit* that we recently developed for non-convex quadratically constrained quadratic programming (QCQP) problems [14]. The first algorithm (B-FPP) is designed for independent and uniformly distributed bounded measurement errors, such as those arising from high-rate quantization. The second (LS-FPP) is designed for i.i.d. Gaussian measurement errors, thereby using a LS criterion. Their performance is measured against state-of-art algorithms and the general Cramér-Rao bound (CRB) for phase retrieval from magnitude measurements in additive Gaussian noise, which is also derived here. Interestingly, only partial CRB results under additional model restrictions and/or different noisy measurement models (e.g., for real- and complex-valued \mathbf{x} [15]-[16], noise added prior to taking the magnitude [17], 2-D Fourier-based measurements [18]) were previously available, despite decades of research in phase retrieval. Simulations show that LS-FPP outperforms the state-of-art and operates close to the CRB. Compact CRB expressions, properties, and insights are obtained by simplifying the CRB in special cases. These can help improve the design of measurement apparatus, by providing a way to score different designs.

Section IV presents a special case where \mathbf{x} is in the form of a linear combination of several Vandermonde vectors, i.e., a harmonic mixture, leading to harmonic retrieval from rank-one quadratic measurements. By predefining an overcomplete frequency basis, sparsity in the frequency domain can be exploited, resulting in modified versions of B-FPP and LS-FPP for sparse phase retrieval. Furthermore, the CRB for frequency estimation is derived for this case.

Section V contains numerical simulations designed to illustrate the performance of the proposed algorithms versus

PhaseCut, *PhaseLift*, WF, and the CRB. Finally, conclusions are drawn in Section VI.

II. PROPOSED ALGORITHMS

In this section, we formulate the phase retrieval problem as non-convex QCQP in two different ways, and derive two corresponding algorithms, B-FPP and LS-FPP, to recover \mathbf{x} .

A. B-FPP Algorithm

In the absence of noise, phase retrieval can be cast as

$$\begin{aligned} \min_{\mathbf{x}} \quad & \|\mathbf{x}\|_2^2 \\ \text{s.t.} \quad & \mathbf{x}^H \mathbf{A}_i \mathbf{x} = y_i, \quad i \in \{1, \dots, M\}, \end{aligned} \quad (7)$$

i.e., a minimum norm solution to a system of quadratic equations in \mathbf{x} . If the equality constraints are consistent, then using the minimum norm to pick a solution can be motivated from a Bayesian perspective, if we assume a zero-mean uncorrelated complex circularly symmetric Gaussian prior on \mathbf{x} .² In practice noise will render the equality constraints in (7) inconsistent, so (7) will not admit any solution. High-resolution uniform scalar quantization of otherwise noiseless quadratic measurements will result in additive quantization noise that is independent across measurements, bounded, and approximately uniformly distributed over the quantization interval. This motivates using interval constraints, as follows:

$$|y_i - \mathbf{x}^H \mathbf{A}_i \mathbf{x}| \leq \epsilon, \quad \forall i. \quad (8)$$

Replacing the constraints in (7) by (8) yields

$$\min_{\mathbf{x}} \quad \|\mathbf{x}\|_2^2 \quad (9a)$$

$$\text{s.t.} \quad \mathbf{x}^H \mathbf{A}_i \mathbf{x} \leq y_i + \epsilon \quad (9b)$$

$$\mathbf{x}^H \mathbf{A}_i \mathbf{x} \geq y_i - \epsilon, \quad \forall i. \quad (9c)$$

It is clear that due to the non-convex constraints in (9c), (9) belongs to the class of non-convex QCQP problems which is NP-hard in general. For $\epsilon = 0$ we recover the ‘standard’ phase retrieval problem, which is NP-hard [19].

To approximately solve (9), we follow [14]. Recall that \mathbf{A}_i is of rank one and it has only one positive eigenvalue. For any \mathbf{z} and \mathbf{x} , we have

$$(\mathbf{x} - \mathbf{z})^H \mathbf{A}_i (\mathbf{x} - \mathbf{z}) \geq 0. \quad (10)$$

Expanding the left-hand side of (10) yields

$$\mathbf{x}^H \mathbf{A}_i \mathbf{x} \geq 2\text{Re}\{\mathbf{z}^H \mathbf{A}_i \mathbf{x}\} - \mathbf{z}^H \mathbf{A}_i \mathbf{z} \quad (11)$$

where $\text{Re}\{\cdot\}$ takes the real part of its argument. Following the rationale in [14], we replace (9c) by

$$2\text{Re}\{\mathbf{z}^H \mathbf{A}_i \mathbf{x}\} + s_i \geq \mathbf{z}^H \mathbf{A}_i \mathbf{z} + y_i - \epsilon \quad (12)$$

where $s_i \geq 0$ is a slack variable. The idea here is that linear restriction turns the non-convex problem into a convex one, but at the risk of infeasibility. The slack variables restore

²Since $\|\mathbf{x}\|_2^2 = \text{tr}(\mathbf{x}\mathbf{x}^H)$, the minimum norm criterion is also reminiscent of semidefinite relaxation of rank minimization.

feasibility, but they should be sparingly used [14]. This leads to the following formulation:

$$\begin{aligned} \min_{\mathbf{x}, \mathbf{s}} \quad & \|\mathbf{x}\|_2^2 + \lambda \sum_{i=1}^M s_i \\ \text{s. t.} \quad & \mathbf{x}^H \mathbf{A}_i \mathbf{x} \leq y_i + \epsilon \\ & 2\text{Re}\{\mathbf{z}^H \mathbf{A}_i \mathbf{x}\} + s_i \geq \mathbf{z}^H \mathbf{A}_i \mathbf{z} + y_i - \epsilon \\ & s_i \geq 0, \forall i \end{aligned} \quad (13)$$

where $\mathbf{s} = [s_1 \ \dots \ s_M]^T$ and the regularization parameter λ balances the objective function and slack penalty term. Starting from an initial \mathbf{z} , we solve a sequence of problems of type (13) to obtain $(\mathbf{x}_k, \mathbf{s}_k)$, starting from some initial (possibly random) \mathbf{z}_1 , and setting $\mathbf{z}_{k+1} = \mathbf{x}_k$. Since the cost function in (13) is independent of k and the solution of the k th iteration is also feasible for the $(k+1)$ th iteration, this will always return a non-increasing cost sequence [14]. In other words, the optimal value of the cost function in each iteration step is non-increasing. It follows that this sequential process will converge in terms of the cost function. The steps for B-FPP are summarized in **Algorithm 1**.

Algorithm 1 B-FPP Algorithm for Phase Retrieval

- 1: **function** $\hat{\mathbf{x}} = \text{B-FPP}(\mathbf{A}, \mathbf{y}, \lambda, \epsilon, \mathbf{z})$
 - 2: **repeat**
 - 3: $\hat{\mathbf{x}} \leftarrow$ solution of (13)
 - 4: $\mathbf{z} = \hat{\mathbf{x}}$
 - 5: **until** a stopping criterion on the cost function of (13) is satisfied
 - 6: **end function**
-

Whereas B-FPP has been motivated from a uniform high-resolution quantization point of view (and indeed matches that noise model), the resulting algorithm can also be used for Gaussian noise, although the choice of ϵ is less obvious in this case. It is instructive to illustrate this by means of an example. Assume \mathbf{x} is uncorrelated zero-mean Gaussian with length $N = 16$, and $M = 80$ measurements are used for signal recovery. 200 Monte-Carlo trials are employed to calculate the mean square error (MSE). In each trial, \mathbf{a}_i , \mathbf{x} and σ_n are fixed, and the noise is generated from a white Gaussian process with mean zero and standard deviation $\sigma_n = 0.4$. Fig. 1 shows the MSE versus ϵ . It is observed that when $\epsilon < 0.4$, B-FPP exhibits relative small MSE. Otherwise, its performance gets worse as ϵ increases. We conclude that B-FPP still works for Gaussian noise, provided $\epsilon \sim \sigma_n$.

B. LS-FPP Algorithm

The B-FPP method requires a user-defined tolerance ϵ to bound the noise perturbation in the constraints, which is difficult to appropriately determine from the magnitude measurements without prior knowledge of the noise standard deviation. More to the point, B-FPP is not tailored for Gaussian noise. In this section we develop *LS-FPP* based on the LS criterion, which is equivalent to maximum likelihood for additive white Gaussian noise. The LS formulation of phase retrieval has been recently considered in [13], but the WF approach does

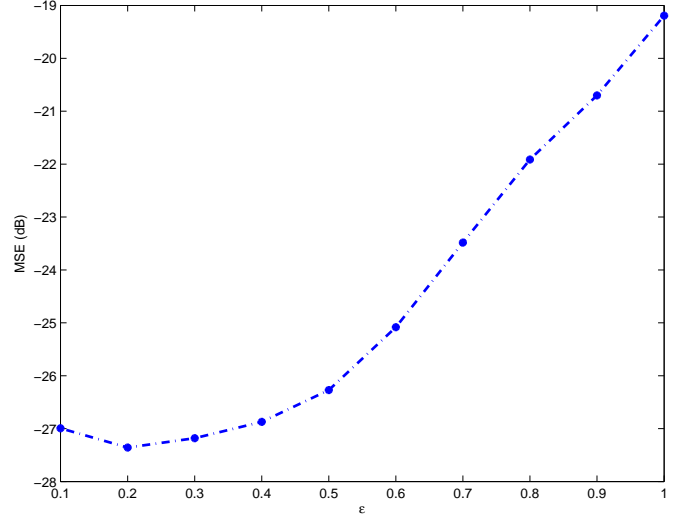


Fig. 1. MSE versus ϵ . ($N = 16$, $M = 80$)

not always work well, as we will show in our simulations in Section V. This is not surprising, of course, since we are dealing with an NP-hard problem. Our contribution here is to recast LS phase retrieval as a non-convex quadratic-plus-linear problem, and then approximate it using FPP. As we will show, our approach gives consistently better approximation results, especially in challenging scenarios, at the cost of additional computational complexity.

The LS formulation for phase retrieval is [13]

$$\min_{\mathbf{x}} \sum_{i=1}^M (y_i - \mathbf{x}^H \mathbf{A}_i \mathbf{x})^2 \quad (14)$$

The first step in our approach is to recast (14) in the following equivalent form

$$\begin{aligned} \min_{\mathbf{w}, \mathbf{x}} \quad & \|\mathbf{w}\|_2^2 \\ \text{s. t.} \quad & \mathbf{x}^H \mathbf{A}_i \mathbf{x} + w_i = y_i, \forall i \end{aligned} \quad (15)$$

where

$$\mathbf{w} = [w_1 \ \dots \ w_M]^T. \quad (16)$$

In order to proceed, we define a $M \times 1$ selection vector \mathbf{e}_i which is the i th column of \mathbf{I}_M , such that

$$w_i = \mathbf{e}_i^T \mathbf{w}. \quad (17)$$

Then the constraints in (15) become

$$\mathbf{x}^H \mathbf{A}_i \mathbf{x} + \mathbf{e}_i^T \mathbf{w} = y_i \quad (18)$$

which can be rewritten as

$$\mathbf{x}^H \mathbf{A}_i \mathbf{x} + \mathbf{e}_i^T \mathbf{w} \leq y_i \quad (19a)$$

$$\mathbf{x}^H \mathbf{A}_i \mathbf{x} + \mathbf{e}_i^T \mathbf{w} \geq y_i. \quad (19b)$$

In a similar manner as we process the non-convex constraints in FPP, (18) can be replaced by (19a) and

$$2\text{Re}\{\mathbf{z}^H \mathbf{A}_i \mathbf{x}\} + \mathbf{e}_i^T \mathbf{w} + s_i \geq y_i + \mathbf{z}^H \mathbf{A}_i \mathbf{z} \quad (20)$$

to obtain the following convex QCQP:

$$\begin{aligned} \min_{\mathbf{x}, \mathbf{w}, \mathbf{s}} \quad & \|\mathbf{w}\|^2 + \lambda \sum_{i=1}^M s_i \\ \text{s. t.} \quad & 2\text{Re}\{\mathbf{z}^H \mathbf{A}_i \mathbf{x}\} + \mathbf{e}_i^T \mathbf{w} + s_i \geq y_i + \mathbf{z}^H \mathbf{A}_i \mathbf{z} \\ & \mathbf{x}^H \mathbf{A}_i \mathbf{x} + \mathbf{e}_i^T \mathbf{w} \leq y_i, \\ & s_i \geq 0, \forall i. \end{aligned} \quad (21)$$

The steps for LS-FPP are summarized in **Algorithm 2**.

Algorithm 2 LS-FPP Algorithm for Phase Retrieval

```

1: function  $\hat{\mathbf{x}} = \text{LS-FPP}(\mathbf{A}, \mathbf{y}, \lambda, \mathbf{z})$ 
2:   repeat
3:      $\hat{\mathbf{x}} \leftarrow$  solution of (21)
4:      $\mathbf{z} = \hat{\mathbf{x}}$ 
5:   until a stopping criterion on the cost function of (21)
        is satisfied
6: end function

```

Remark 1: The problems in (13) and (21) are convex and can be solved via interior point methods [20]-[21]. The worst-case complexity of solving (13) and (21) are $\mathcal{O}((N+2M)^{3.5})$ and $\mathcal{O}((N+3M)^{3.5})$, respectively. Moreover, few outer iterations of B-FPP or LS-FPP are usually needed, so that the overall approximation is often manageable for moderate N .

III. CRAMÉR-RAO BOUND FOR PHASE RETRIEVAL

In this section, we derive the CRB for phase retrieval for measurements contaminated by additive white Gaussian noise *after* magnitude squaring. Let us summarize the (surprisingly scant) prior work on the CRB for phase retrieval. Balan [15], [16] has derived the Fisher Information Matrix (FIM) for the model in (6) for complex \mathbf{x} , and noted that it is singular. Attributing this to the lack of global phase identifiability, he proposed using side information about \mathbf{x} to compute the CRB. Identifiability neither implies nor is implied by a finite FIM [22], so we make no such assumption, and use the pseudoinverse instead, as detailed later. In the case of real \mathbf{x} , Balan's result is valid only for real measurement vectors. Balan also derived [17] the FIM for white Gaussian noise added *prior* to taking the magnitude square, i.e., $y_i = |\mathbf{a}_i^H \mathbf{x} + n_i|^2$, which is different from our model in (1). We also note [18], where the CRB has been derived for a 2-D phase retrieval model with 2-D Fourier measurements. Unlike these previous works, we aim at deriving a general CRB for phase retrieval of complex-valued \mathbf{x} from (6), when n_i is white Gaussian. Note that the CRB for real-valued \mathbf{x} is a special case, and many other (non-Gaussian) noise probability density functions possessing everywhere continuous first and second derivatives can be easily handled – as the corresponding CRB only differs by a noise distribution-specific shape factor [23].

A. CRB for Complex-Valued \mathbf{x}

The following theorem presents a closed-form expression for the CRB of complex-valued \mathbf{x} under white Gaussian noise.

Theorem 3.1: For $\mathbf{x} \in \mathbb{C}^N$, the CRB for the phase retrieval model in (6) is

$$\text{CRB}_c = \mathbf{F}_c^\dagger \quad (22)$$

where the Fisher information matrix (FIM) is given by

$$\mathbf{F}_c = \frac{4}{\sigma_n^2} \mathbf{G}_c \mathbf{G}_c^T \quad (23)$$

with

$$\mathbf{G}_c = \begin{bmatrix} \text{Re}\{\mathbf{A}_1 \mathbf{x}\} & \cdots & \text{Re}\{\mathbf{A}_M \mathbf{x}\} \\ \text{Im}\{\mathbf{A}_1 \mathbf{x}\} & \cdots & \text{Im}\{\mathbf{A}_M \mathbf{x}\} \end{bmatrix}. \quad (24)$$

Proof: See Appendix A. ■

We note that \mathbf{F}_c for complex \mathbf{x} is always singular, with rank deficit equal to one. When the FIM is rank deficient, its pseudo-inverse is a valid lower bound on the MSE of any unbiased estimator [24], [25], albeit this bound is generally looser than the usual CRB [26]. Perhaps surprisingly, this ‘optimistic’ bound is often attainable in practice and therefore predictive of optimal estimator performance – see [27] and our simulations that follow. Strictly speaking, the pseudo-inverse of a singular FIM is not the usual CRB, and some researchers distinguish the two bounds; but this is a technical detail with little practical consequence, so we will refer to the resultant bound as the CRB.

We intuitively expect a reduced bound when more measurements are added. The following theorem shows that this is indeed true.

Proposition 3.2: For given \mathbf{x} and fixed σ_n , the CRB in (22) decreases as more measurements are made available:

$$\text{CRB}_c(\mathbf{A}(:, 1 : M + 1)) \leq \text{CRB}_c(\mathbf{A}(:, 1 : M)), \quad (25)$$

where $\mathbf{A}(:, \ell : r)$ is (Matlab notation for) the submatrix of \mathbf{A} comprising columns ℓ to r inclusive.

Proof: To prove (25), we first define $\mathbf{F}_c(M)$ and $\mathbf{F}_c(M+1)$ as the FIMs for M and $(M+1)$ measurements, respectively. Then, we have

$$\mathbf{F}_c(M+1) = \mathbf{F}_c(M) + \frac{4}{\sigma_n^2} \mathbf{g}_{c,M+1} \mathbf{g}_{c,M+1}^T \quad (26)$$

where

$$\mathbf{g}_{c,M+1} = \begin{bmatrix} \text{Re}\{\mathbf{A}_{M+1} \mathbf{x}\} \\ \text{Im}\{\mathbf{A}_{M+1} \mathbf{x}\} \end{bmatrix}. \quad (27)$$

It is seen that the second term in (26) is positive semidefinite. By taking the pseudo-inverse of (26), (25) is established straightforwardly. ■

To make the above results more intuitive, we study the CRB for the special case where $N = 1$. In this case, we have $\mathbf{A}_i = |a_i|^2$, $\mathbf{x} = x_1$ and

$$\mathbf{G}_c = \begin{bmatrix} |a_1|^2 \text{Re}\{x_1\} & \cdots & |a_M|^2 \text{Re}\{x_1\} \\ |a_1|^2 \text{Im}\{x_1\} & \cdots & |a_M|^2 \text{Im}\{x_1\} \end{bmatrix}. \quad (28)$$

The \mathbf{F}_c is then simplified as

$$\mathbf{F}_c = \frac{4}{\sigma_n^2} \sum_{i=1}^M |a_i|^4 \tilde{\mathbf{F}}_c \quad (29)$$

where

$$\tilde{\mathbf{F}}_c = \begin{bmatrix} (\operatorname{Re}\{x_1\})^2 & \operatorname{Re}\{x_1\}\operatorname{Im}\{x_1\} \\ \operatorname{Im}\{x_1\}\operatorname{Re}\{x_1\} & (\operatorname{Im}\{x_1\})^2 \end{bmatrix}. \quad (30)$$

Since $\tilde{\mathbf{F}}_c$ is a symmetric matrix with rank one only, according to [28], its pseudo-inverse can be calculated via the eigenvalue decomposition (EVD):

$$\tilde{\mathbf{F}}_c^\dagger = \frac{\tilde{\mathbf{F}}_c}{|x_1|^4} \quad (31)$$

where $|x_1| = \sqrt{(\operatorname{Re}\{x_1\})^2 + (\operatorname{Im}\{x_1\})^2}$. Substituting (31) into (29) yields

$$\mathbf{F}_c^\dagger = \frac{\tilde{\mathbf{F}}_c}{4M \cdot \text{SNR}} \quad (32)$$

where

$$\text{SNR} = \frac{\sum_{i=1}^M |a_i^* x_1|^4}{M \sigma_n^2} = \frac{\sum_{i=1}^M |a_i|^4}{M \sigma_n^2} \cdot |x_1|^4 \quad (33)$$

Thus, summing the diagonal elements of \mathbf{F}_c^\dagger produces the CRB, i.e.,

$$\text{CRB}_c = \frac{|x_1|^2}{4M \cdot \text{SNR}} \quad (34)$$

which shows that for a given SNR, the CRB decreases as M increases, and for a fixed value of M , the CRB decreases as SNR increases.

B. CRB for Real-Valued \mathbf{x}

Theorem 3.3: For $\mathbf{x} \in \mathbb{R}^N$, the CRB for the phase retrieval model in (6) is given as

$$\text{CRB}_r = \mathbf{F}_r^{-1} \quad (35)$$

where $(\cdot)^{-1}$ denotes the inverse and

$$\mathbf{F}_r = \frac{4}{\sigma_n^2} \mathbf{G}_r \mathbf{G}_r^T \quad (36)$$

with

$$\mathbf{G}_r = [\operatorname{Re}\{\mathbf{A}_1\}\mathbf{x} \quad \cdots \quad \operatorname{Re}\{\mathbf{A}_M\}\mathbf{x}]. \quad (37)$$

Proof: See (58)-(72) in Appendix A. ■

Note that \mathbf{F}_r in (36) has full rank. Also note that, unlike the complex case which involves an inherently unresolvable global phase ambiguity, there is only sign ambiguity that is inherent in the real-valued case. Moreover, the CRB in Theorem 3.3 has similar properties as the one in Theorem 1. For example, for fixed σ_n , additional measurements yield lower CRB, i.e.,

$$\text{CRB}_r(\mathbf{A}(:, 1 : M + 1)) \leq \text{CRB}_r(\mathbf{A}(:, 1 : M)). \quad (38)$$

By using similar derivations from (28) to (34), we can prove that when $N = 1$, the CRB for real-valued \mathbf{x} is reduced to

$$\text{CRB}_r = \frac{x_1^2}{4M \cdot \text{SNR}} \quad (39)$$

which has exactly the same expression as (34) since $x_1^2 = |x_1|^2$ when \mathbf{x} is real.

IV. HARMONIC RETRIEVAL FROM RANK-ONE QUADRATIC MEASUREMENTS

A. Signal Model

In this section, we consider a special case of (6) when \mathbf{x} is a linear combination of L Vandermonde vectors where each vector contains a single frequency, i.e.,

$$\mathbf{x} = \sum_{\ell=1}^L \gamma_\ell \mathbf{v}(\omega_\ell) \quad (40)$$

Here, ω_ℓ and γ_ℓ stand for the ℓ th unknown frequency and complex amplitude, respectively, and

$$\mathbf{v}(\omega_\ell) = [e^{j\omega_\ell} \quad \cdots \quad e^{jN\omega_\ell}]^T. \quad (41)$$

The main problem here is to estimate the frequencies $\{\omega_1 \cdots \omega_L\}$ from \mathbf{y} . Classical line spectra estimators such as MUSIC and ESPRIT assume that \mathbf{x} is sampled directly and there is no phase noise. What if we observe *generalized samples*, i.e., linear combinations of the elements of \mathbf{x} , and these are subject to phase noise, i.e., $\mathbf{s} = \operatorname{diag}(\mathbf{u})\mathbf{A}^H \mathbf{x}$, where u_i models phase noise in the i -th measurement ($|u_i| = 1$), which could arise, e.g., due to phase offsets when different measurements are collected by different sensors in a network sensing scenario. In this case, the phase of \mathbf{s} is clearly uninformative, and we might as well get rid of it by working with $|\mathbf{s}|$ - see also [29]. This yields a phase retrieval problem where the unknown \mathbf{x} possesses harmonic structure. Can we adapt our algorithms and bounds to account for this structure?

B. Sparse B-FPP and LS-FPP

We propose to adapt B-FPP and LS-FPP using sparse regression with an overcomplete Vandermonde dictionary. Let $\tilde{\mathbf{V}} \in \mathbb{C}^{N \times P}$ be a known overcomplete basis parametrized by $\{\tilde{\omega}_1 \cdots \tilde{\omega}_P\}$. More specifically, $\tilde{\mathbf{V}}$ can be expressed as

$$\tilde{\mathbf{V}} = [\mathbf{v}(\tilde{\omega}_1) \quad \cdots \quad \mathbf{v}(\tilde{\omega}_P)]. \quad (42)$$

Note that P should be much larger than the number of active frequencies L . Assuming a sufficiently dense grid, \mathbf{x} can be approximated as

$$\mathbf{x} \approx \tilde{\mathbf{V}}\tilde{\mathbf{x}} \quad (43)$$

where $\tilde{\mathbf{x}} \in \mathbb{C}^P$ is L -sparse. Substituting (43) into (6) yields

$$y_i \approx |\mathbf{b}_i^H \tilde{\mathbf{x}}|^2 + n_i, \quad \forall i \quad (44)$$

where

$$\mathbf{b}_i = \tilde{\mathbf{V}}^H \mathbf{a}_i. \quad (45)$$

The problem of frequency estimation has been converted to sparse spectrum ($\tilde{\mathbf{x}}$) estimation. An ideal description of sparsity is the ℓ_0 -norm $\|\mathbf{x}\|_0$, i.e., the number of nonzero entries in \mathbf{x} . However, this yields a ‘doubly NP-hard’ problem. In recent years, numerous approximations have been developed such as ℓ_1 and ℓ_p ($p < 1$) relaxations [30]-[31], to replace

the ℓ_0 -norm. For sparse B-FPP, we can use ℓ_1 relaxation as follows

$$\begin{aligned} \min_{\tilde{\mathbf{x}}, \mathbf{s}} \quad & \|\tilde{\mathbf{x}}\|_2^2 + \lambda_1 \|\tilde{\mathbf{x}}\|_1 + \lambda_2 \sum_{i=1}^M s_i \\ \text{s. t.} \quad & 2\text{Re}\{\mathbf{z}^H \mathbf{B}_i \tilde{\mathbf{x}}\} + s_i \geq \mathbf{z}^H \mathbf{B}_i \mathbf{z} + y_i - \epsilon \\ & \tilde{\mathbf{x}}^H \mathbf{B}_i \tilde{\mathbf{x}} \leq y_i + \epsilon \\ & s_i \geq 0, \quad \forall i \end{aligned} \quad (46)$$

where $\mathbf{B}_i = \mathbf{b}_i \mathbf{b}_i^H \in \mathbb{C}^{P \times P}$, $\tilde{\mathbf{x}} \in \mathbb{C}^P$ and $\mathbf{z} \in \mathbb{C}^P$. For sparse LS-FPP, we likewise have

$$\begin{aligned} \min_{\tilde{\mathbf{x}}, \mathbf{w}, \mathbf{s}} \quad & \|\mathbf{w}\|^2 + \lambda_1 \|\tilde{\mathbf{x}}\|_1 + \lambda_2 \sum_{i=1}^M s_i \\ \text{s. t.} \quad & 2\text{Re}\{\mathbf{z}^H \mathbf{B}_i \tilde{\mathbf{x}}\} + \mathbf{e}_i^T \mathbf{w} + s_i \geq \mathbf{z}^H \mathbf{B}_i \mathbf{z} + y_i \\ & \tilde{\mathbf{x}}^H \mathbf{B}_i \tilde{\mathbf{x}} + \mathbf{e}_i^T \mathbf{w} \leq y_i, \\ & s_i \geq 0, \quad \forall i. \end{aligned} \quad (47)$$

Remark 2: Similar to **Algorithm 1** and **Algorithm 2** for ‘plain’ phase retrieval, (46) and (47) can be solved repeatedly using the previously obtained $\tilde{\mathbf{x}}$ to obtain a new supporting point \mathbf{z} . Also note that sparse B-FPP and sparse LS-FPP are not limited to harmonic retrieval – they are directly applicable to other cases where \mathbf{x} admits a sparse representation in a known dictionary.

C. CRB for Harmonic Retrieval from Quadratic Measurements

When \mathbf{x} is modeled as a sum of a few harmonics, the CRB is associated to the unknown frequencies ω_ℓ and complex amplitudes γ_ℓ rather than \mathbf{x} . The corresponding CRB is provided in the following theorem.

Theorem 4.1: If $\mathbf{x} \in \mathbb{C}^N$ is a superposition of L Vandermonde vectors as in (40), the CRB is

$$\text{CRB}_v = \mathbf{F}_v^\dagger \quad (48)$$

where

$$\mathbf{F}_v = \frac{4}{\sigma_n^2} \mathbf{G}_v \mathbf{G}_v^T \quad (49)$$

with

$$\mathbf{G}_v = \begin{bmatrix} \text{Re}\{\mathbf{X}^H \mathbf{A}_1 \mathbf{x}\} & \cdots & \text{Re}\{\mathbf{X}^H \mathbf{A}_M \mathbf{x}\} \\ \text{Re}\{\mathbf{V}^H \mathbf{A}_1 \mathbf{x}\} & \cdots & \text{Re}\{\mathbf{V}^H \mathbf{A}_M \mathbf{x}\} \\ \text{Im}\{\mathbf{V}^H \mathbf{A}_1 \mathbf{x}\} & \cdots & \text{Im}\{\mathbf{V}^H \mathbf{A}_M \mathbf{x}\} \end{bmatrix} \quad (50)$$

$$\mathbf{X} = \begin{bmatrix} \gamma_1 \frac{\partial \mathbf{v}_1}{\partial \omega_1} & \cdots & \gamma_L \frac{\partial \mathbf{v}_L}{\partial \omega_L} \end{bmatrix} \quad (51)$$

$$\mathbf{V} = [\mathbf{v}(\omega_1) \quad \cdots \quad \mathbf{v}(\omega_L)] \quad (52)$$

$$\frac{\partial \mathbf{v}_\ell}{\partial \omega_\ell} = [j e^{j\omega_\ell} \quad \cdots \quad j N e^{jN\omega_\ell}]^T. \quad (53)$$

Proof: See Appendix B. ■

V. SIMULATION RESULTS

We present simulations of the two proposed methods and compare them with WF [13], PhaseLift [8] and PhaseCut [12] in this section. For faster convergence, B-FPP and LS-FPP are initialized by the output of PhaseLift. The stopping criterion used in both B-FPP and LS-FPP is $\|\mathbf{z}_k - \hat{\mathbf{x}}\|_2^2 \leq 10^{-5}$ or a maximum number of iterations, set to 10. The measurement vectors $\{\mathbf{a}_i\}_{i=1}^M$ are generated from a complex normal distribution, except where noted otherwise (in two experiments where we use masked Fourier measurement vectors). The noise is assumed to be white Gaussian with mean zero and variance σ_n^2 . Furthermore, the SNR is defined as

$$\text{SNR} = \frac{\sum_{i=1}^M |\mathbf{a}_i^H \mathbf{x}|^4}{M \sigma_n^2}. \quad (54)$$

In the following tests, we consider two types of signals, i.e., complex-valued and real-valued \mathbf{x} , to examine the performance of our algorithms. The signal \mathbf{x} is deterministic and fixed throughout all Monte-Carlo trials, with the following forms:

- Complex-valued case: \mathbf{x} is a sampled version of $\exp((j0.4\pi - 0.3)t)$, $t \in [0, 10]$ comprising 32 uniform samples.
- Real-valued case: \mathbf{x} consists of 32 uniform samples of $\sin(0.4\pi t)$, $t \in [0, 10]$.

A. CRB versus SNR

As a first sanity check, Fig. 2 plots the CRB as a function of SNR for $M = 3N, 5N$, and $10N$ for the complex-valued signal (top) and the real-valued signal (bottom), for $N = 32$. It is seen that as predicted by Theorems 3.1 and 3.3, the bound on the standard deviation of the estimated \mathbf{x} decreases as SNR increases. As expected, we also find that the CRB associated to a larger M produces a smaller bound on the standard deviation, which validates our analytical results in (25) and (38). As another check, we set $N = 1$ and compare the complex-valued and real-valued CRBs with the closed-form analytical results in (34) and (39), respectively.

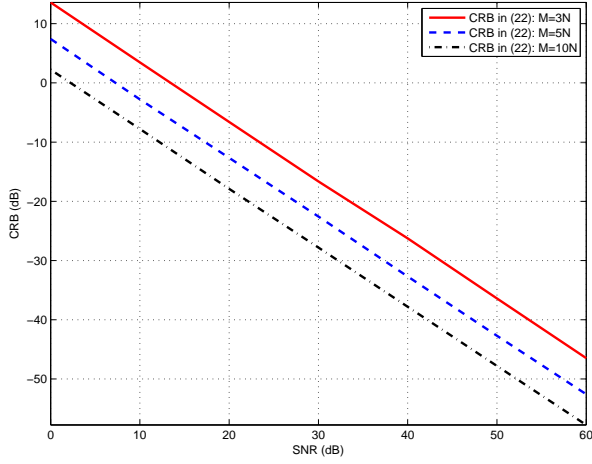
B. Performance Comparison for Complex-valued \mathbf{x}

We now compare the performance of B-FPP and LS-FPP with PhaseLift, PhaseCut³ and WF [13]. For PhaseLift, PhaseCut, and WF, we used publicly available code⁴. We used the LS version of PhaseLift that is appropriate for additive Gaussian noise.

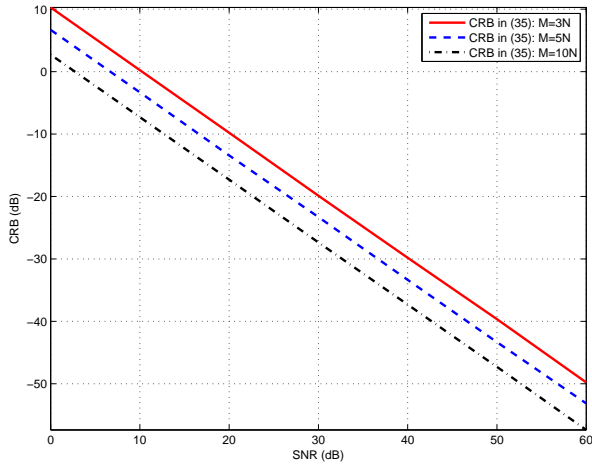
To begin, let us illustrate the recovery performance of FPP and LS-FPP by means of example. We consider the complex signal in a) with length $N = 32$, and $M = 5N = 160$ measurements. The SNR is 20 dB. It is shown in Fig. 4 that our approach can accurately recover \mathbf{x} (for illustration purposes,

³PhaseCut works with $\sqrt{\mathbf{y}}$; \mathbf{y} can have negative elements at low SNR, so we use $\text{Re}\{\sqrt{\mathbf{y}}\}$ for PhaseCut. Also note that, due to the nonlinear transformation, noise will no longer be additive Gaussian for PhaseCut, which matches a different measurement model, namely $z_i = |\mathbf{a}_i^H \mathbf{x}| + n_i$.

⁴Downloaded from http://www-bcf.usc.edu/~soltanol/PhaseRetrieval_CDP.zip, <http://www.cmap.polytechnique.fr/scattering/code/phasercovery.zip>, and <http://www-bcf.usc.edu/~soltanol/WFcode.html>, respectively.



(a) Complex-valued case



(b) Real-valued case

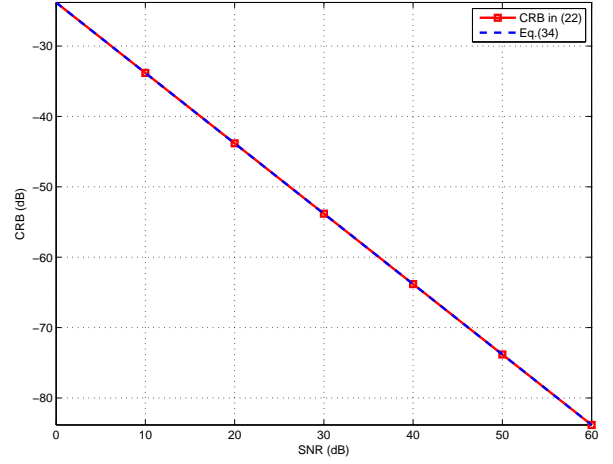
Fig. 2. CRB versus SNR for different M .

we remove the global phase ambiguity after signal recovery). For B-FPP, ϵ is set equal to the standard deviation of the noise, for all our experiments.

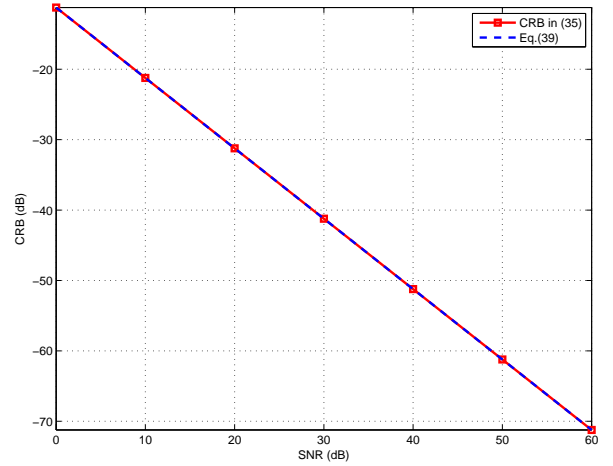
Next, we compare the MSE estimation performance and probability of resolution of all methods as a function of SNR, using $N = 32$, $M = 160$, and 50 Monte-Carlo trials. The signal is considered to be resolved if the following criterion is satisfied after fixing the global phase ambiguity:

$$\|\hat{\mathbf{x}} - \mathbf{x}\|_2 \leq 0.1,$$

Otherwise we declare an outage. The CRB for complex-valued \mathbf{x} in Theorem 1 is also included as a benchmark. Fig. 5(a) depicts the MSE results for Gaussian measurements, from which we can observe that the LS-FPP followed by B-FPP achieves the best performance and both of them outperform WF, PhaseLift and PhaseCut when SNR is larger than 10 dB. The relatively large MSE of WF is mainly caused by occasional outages, as can be verified from Fig. 5(b), where the probability of resolution for WF, PhaseCut and PhaseLift is 95%, 98% and 60%, respectively, at high SNR. We also included a curve ‘WF without outages’ to show the performance of WF after discarding trials where WF resulted in



(a) Complex-valued case



(b) Real-valued case

Fig. 3. CRB versus SNR for $N = 1$.

outage. In Fig. 5(a), we can see that the performance of both LS-FPP and WF without outages attain the CRB when SNR > 20 dB. Similar results can also be found in Fig. 6, where 4 masked Fourier measurements are used. Here, the masked Fourier matrix has the form of

$$\mathbf{A}^H = \begin{bmatrix} \mathbf{F}\mathbf{D}_1 \\ \mathbf{F}\mathbf{D}_2 \\ \mathbf{F}\mathbf{D}_3 \\ \mathbf{F}\mathbf{D}_4 \end{bmatrix} \quad (55)$$

where \mathbf{F} is a $N \times N$ Fourier matrix and \mathbf{D}_i is a $N \times N$ diagonal masking matrix with its diagonal entries generated by $b_1 b_2$, whereby b_1 and b_2 are independent and distributed as [13]

$$b_1 = \begin{cases} 1 & \text{with prob. 0.25} \\ -1 & \text{with prob. 0.25} \\ -j & \text{with prob. 0.25} \\ j & \text{with prob. 0.25} \end{cases} \quad (56)$$

and

$$b_2 = \begin{cases} \sqrt{2}/2 & \text{with prob. 0.8} \\ \sqrt{3} & \text{with prob. 0.2.} \end{cases} \quad (57)$$

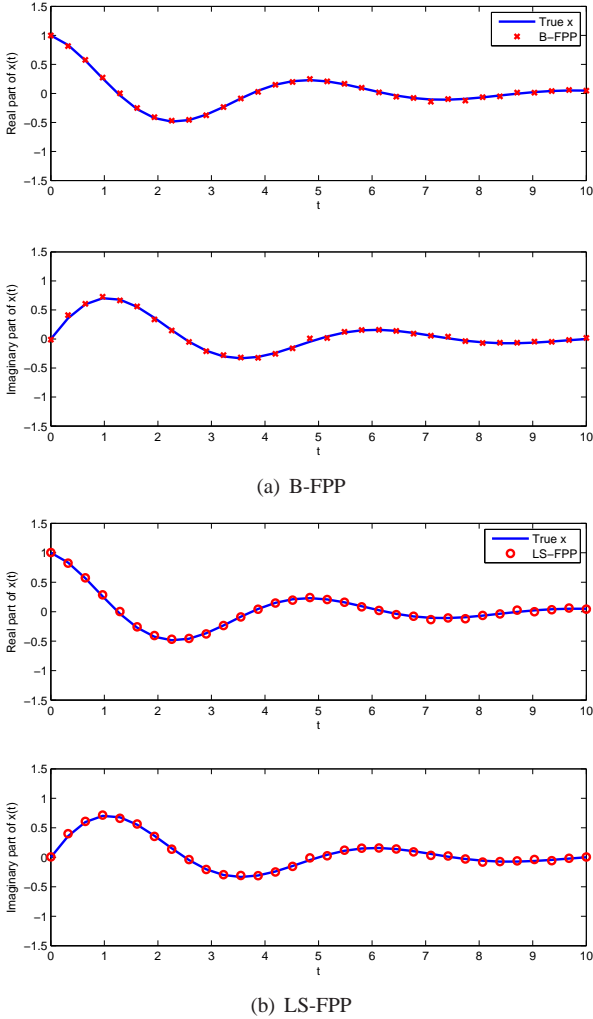


Fig. 4. Signal recovery of complex-valued \mathbf{x} .

C. Performance Comparison for Real-Valued \mathbf{x}

We now study the performance of all algorithms in the real-valued case. All the parameters are the same as for Fig. 4, except that the signal here is assumed to be the real-valued sinusoid in b). It is seen in Fig. 7 that both B-FPP and LS-FPP can successfully recover \mathbf{x} . To obtain further insight into the role of SNR, Fig. 8(a) and 9(a) depict the MSE performance versus SNR, where it can be seen that WF does not work very well, but PhaseLift and PhaseCut provide much better results than in the complex case (note that here we have essentially half the number of unknowns). The LS-FPP and WF without outages merge together and attain the CRB when SNR > 20 dB. Regarding the probability of resolution, only the WF cannot achieve 100% while the other algorithms can successfully resolve \mathbf{x} in the high SNR regime.

D. Performance Comparison for Harmonic Retrieval from Rank-one Quadratic Measurements

Finally, we consider a scenario where \mathbf{x} has the form of a 1-D harmonic model. Assume that there are two frequencies contained in \mathbf{x} , i.e.,

$$\mathbf{x} = \mathbf{v}(\omega_1) + \mathbf{v}(\omega_2).$$

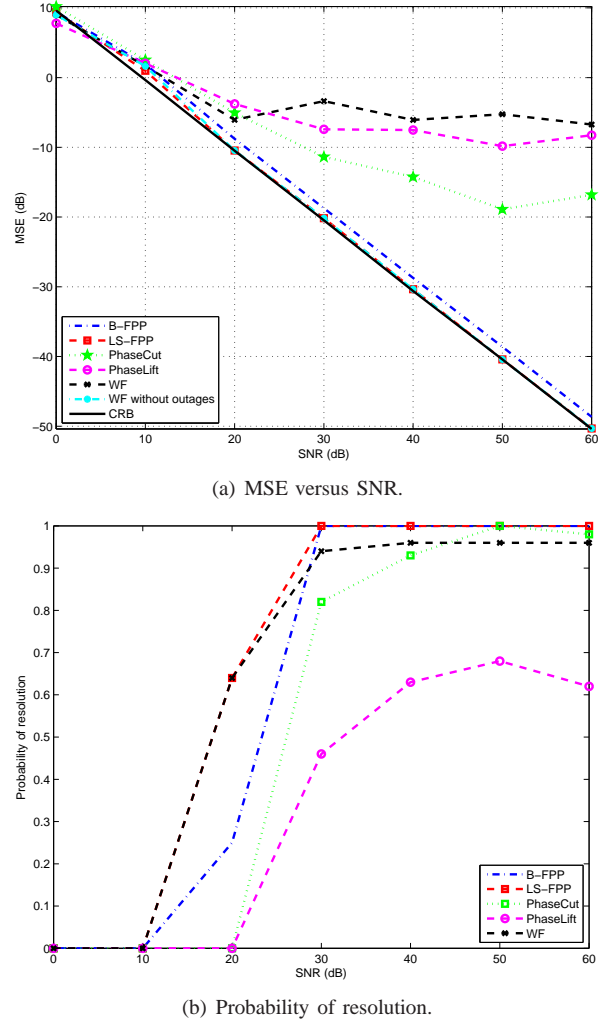
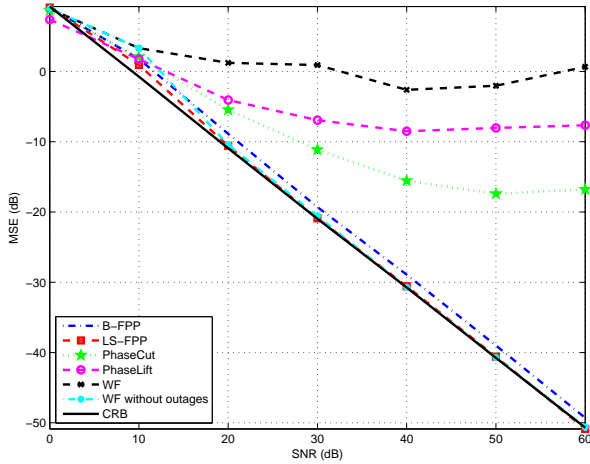


Fig. 5. Performance comparison for complex-valued \mathbf{x} with Gaussian measurements.

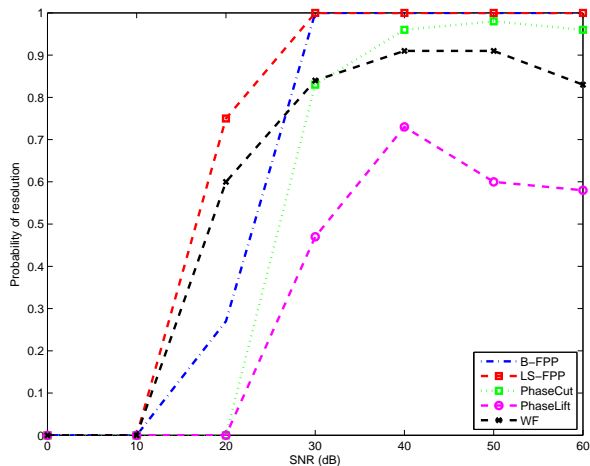
We study the CRB in (53) as a function of SNR. In this example, we assume that $N = 8$ and $M = 40$. Fig. 10 plots two CRB curves corresponding to widely-spaced frequencies ($\omega_1 = -0.15\pi$ and $\omega_2 = 0.15\pi$) and closely-spaced frequencies ($\omega_1 = -0.05\pi$ and $\omega_2 = 0.05\pi$). As expected, the CRB for closely-spaced frequencies is larger than that for widely-spaced ones. Fig. 11 plots the pseudo power spectra, i.e., $\hat{\mathbf{x}}$, obtained by sparse B-FPP and sparse LS-FPP. In this example, the parameters are $\omega_1 = -0.15\pi$, $\omega_2 = 0.15\pi$, $N = 8$, $M = 16$ and SNR = 30 dB. The dictionary with length 101 is defined by uniformly dividing a $[-\pi/2, \pi/2]$ frequency sector. It is observed from Fig. 11 that sparse LS-FPP has two distinct peaks around the true ω while the sparse B-FPP has a small bias on the estimate of ω_2 .

VI. CONCLUSION

The problem of phase retrieval has been revisited from a non-convex QCQP point of view. Building upon recent work on feasible point pursuit for non-convex QCQP problems, two novel algorithms were developed for phase retrieval from noisy measurements: B-FPP and LS-FPP. B-FPP is designed



(a) MSE versus SNR.



(b) Probability of resolution.

Fig. 6. Performance comparison for complex-valued \mathbf{x} with 4 masked Fourier measurements.

for uniform additive noise, such as quantization noise introduced by high-resolution uniform quantization. LS-FPP is matched to white Gaussian noise that is added after taking the magnitude squared of the linear measurements, such as analog transmission noise. For the latter model, the Cramér-Rao bound was also derived and studied. Simulations suggest that B-FPP and LS-FPP attain state-of-art performance, and LS-FPP outperforms all earlier methods and comes very close to the CRB under certain conditions (depending on the SNR, and the type and number of measurements relative to the signal dimension). It was also shown that what apparently hurts the average performance of some of the most competitive algorithms is outages, even when they are rare. LS-FPP exhibits the best outage performance among all algorithms considered, including WF, which seems to be quite sensitive to outages, especially for systematic (as opposed to i.i.d. Gaussian) measurement vectors, which throw off its initialization. Variations of B-FPP and LS-FPP (and the corresponding CRB) for harmonic retrieval from rank-one quadratic measurements were also developed and illustrated in simulations. The drawback of B-FPP and LS-FPP is their

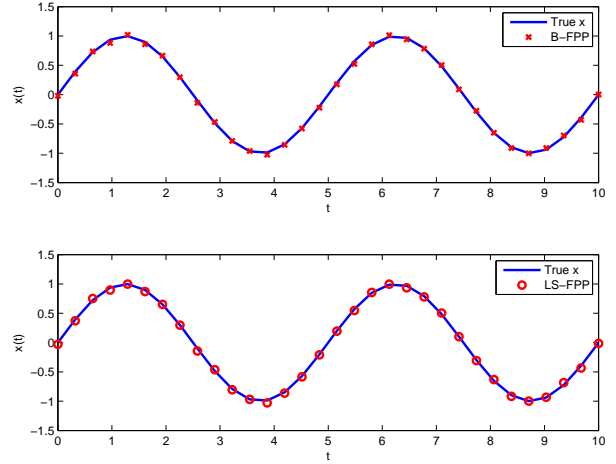


Fig. 7. Signal recovery of real-valued \mathbf{x} .

relatively high computational complexity, especially compared to WF. Ways of bringing down this complexity, possibly using variations of the initialization WF scheme, will be the subject of future work.

APPENDIX A PROOF OF THEOREM 3.1

The CRB states that the variance of any unbiased estimator is at least as high as the inverse of the FIM. To determine the CRB, we should first calculate the FIM and then take its inverse. The likelihood function for the data model for complex \mathbf{x} is

$$p(\mathbf{y}; \mathbf{x}) = \prod_{i=1}^M \frac{1}{\sqrt{2\pi\sigma_n^2}} \exp \left\{ -\frac{(y_i - \mathbf{x}^H \mathbf{A}_i \mathbf{x})^2}{2\sigma_n^2} \right\}. \quad (58)$$

Hence, the log-likelihood function can be written as

$$\ln p(\mathbf{y}; \mathbf{x}) = -\frac{M}{2} \ln(2\pi\sigma_n^2) - \frac{1}{2\sigma_n^2} \sum_{i=1}^M (y_i - \mathbf{x}^H \mathbf{A}_i \mathbf{x})^2. \quad (59)$$

The vector of unknown parameters for complex \mathbf{x} is

$$\boldsymbol{\beta} = [\text{Re}\{x_1\} \cdots \text{Re}\{x_N\} \text{Im}\{x_1\} \cdots \text{Im}\{x_N\}]^T \quad (60)$$

Thus, the FIM can be expressed as

$$\mathbf{F}_c = \begin{bmatrix} \mathbf{F}_{rr} & \mathbf{F}_{ri} \\ \mathbf{F}_{ir} & \mathbf{F}_{ii} \end{bmatrix} \quad (61)$$

where the (m, n) entry of the FIM is given by

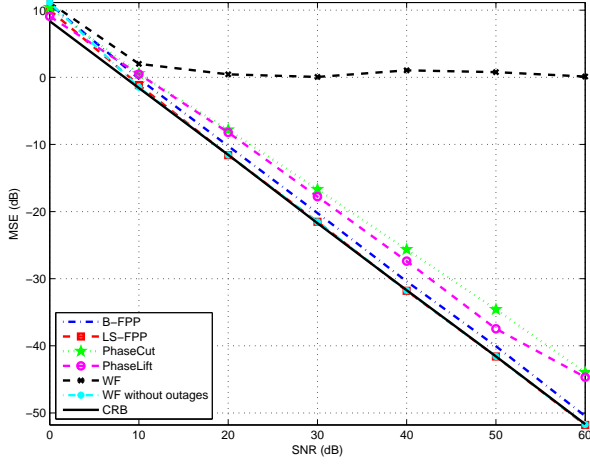
$$[\mathbf{F}_c]_{m,n} = -\mathbb{E} \left[\frac{\partial^2 \ln p(\mathbf{y}; \mathbf{x})}{\partial \beta_m \partial \beta_n} \right] \quad (62)$$

and

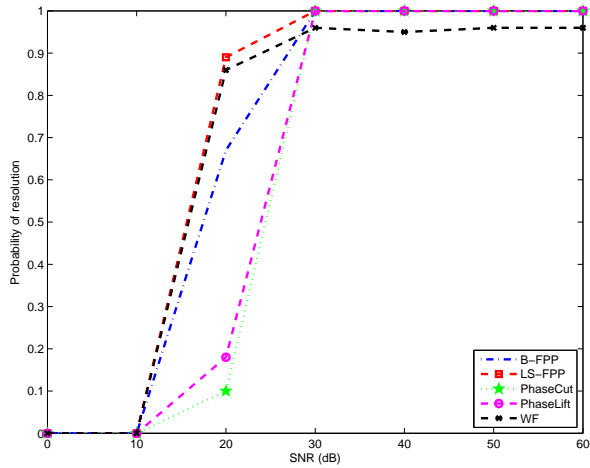
$$[\mathbf{F}_{rr}]_{m,n} = -\mathbb{E} \left[\frac{\partial^2 \ln p(\mathbf{y}; \mathbf{x})}{\partial \text{Re}\{x_m\} \partial \text{Re}\{x_n\}} \right] \quad (63)$$

$$[\mathbf{F}_{ri}]_{m,n} = -\mathbb{E} \left[\frac{\partial^2 \ln p(\mathbf{y}; \mathbf{x})}{\partial \text{Re}\{x_m\} \partial \text{Im}\{x_n\}} \right] \quad (64)$$

$$[\mathbf{F}_{ir}]_{m,n} = -\mathbb{E} \left[\frac{\partial^2 \ln p(\mathbf{y}; \mathbf{x})}{\partial \text{Im}\{x_m\} \partial \text{Re}\{x_n\}} \right] \quad (65)$$



(a) MSE versus SNR.



(b) Probability of resolution.

Fig. 8. Performance comparison for real-valued \mathbf{x} with Gaussian measurements.

$$[\mathbf{F}_{ii}]_{m,n} = -\mathbb{E}\left[\frac{\partial^2 \ln p(\mathbf{y}; \mathbf{x})}{\partial \text{Im}\{x_m\} \partial \text{Im}\{x_n\}}\right] \quad (66)$$

with $\mathbb{E}[\cdot]$ being the expectation operator. The first-order derivative of $\ln p(\mathbf{y}; \mathbf{x})$ with respect to $\text{Re}\{x_m\}$ is

$$\frac{\partial \ln p(\mathbf{y}; \mathbf{x})}{\partial \text{Re}\{x_m\}} = \frac{1}{\sigma_n^2} \sum_{i=1}^M \left((y_i - \mathbf{x}^H \mathbf{A}_i \mathbf{x}) \frac{\partial \mathbf{x}^H \mathbf{A}_i \mathbf{x}}{\partial \text{Re}\{x_m\}} \right). \quad (67)$$

To obtain (67), we first calculate

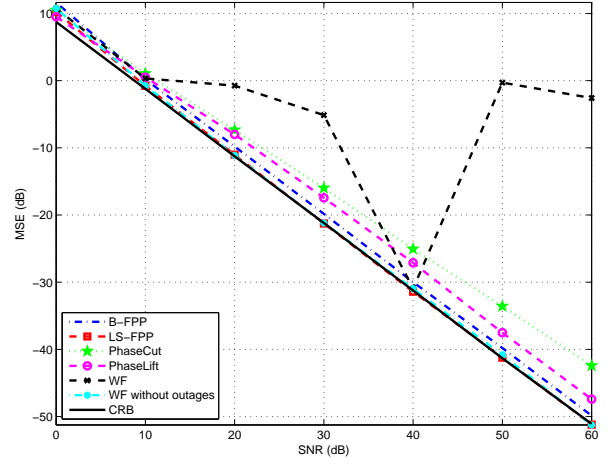
$$\begin{aligned} \frac{\partial \mathbf{x}^H \mathbf{A}_i \mathbf{x}}{\partial \text{Re}\{x_m\}} &= \sum_{k=1}^N [\mathbf{A}_i]_{m,k} x_k + \sum_{l=1}^N x_l^* [\mathbf{A}_i]_{l,m} \\ &= 2\text{Re}\{\mathbf{A}_i(m, :)\mathbf{x}\}. \end{aligned} \quad (68)$$

Substituting (68) into (67), we obtain

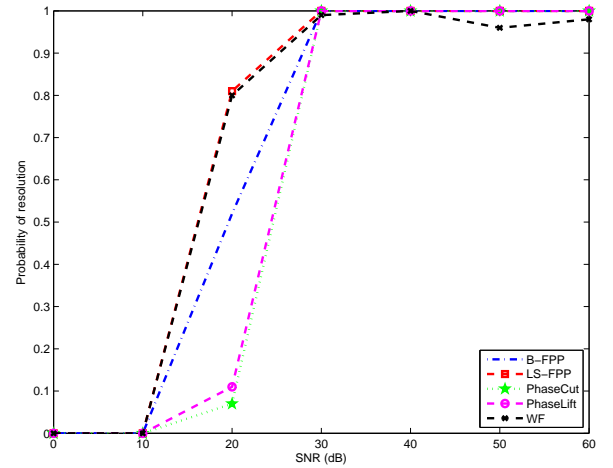
$$\frac{\partial \ln p(\mathbf{y}; \mathbf{x})}{\partial \text{Re}\{x_m\}} = \frac{2}{\sigma_n^2} \sum_{i=1}^M (y_i - \mathbf{x}^H \mathbf{A}_i \mathbf{x}) \text{Re}\{\mathbf{A}_i(m, :)\mathbf{x}\}. \quad (69)$$

Then the second-order partial derivative of $\ln p(\mathbf{y}; \mathbf{x})$ is

$$\frac{\partial^2 \ln p(\mathbf{y}; \mathbf{x})}{\partial \text{Re}\{x_m\} \partial \text{Re}\{x_n\}}$$



(a) MSE versus SNR.



(b) Probability of resolution.

Fig. 9. Performance comparison for real-valued \mathbf{x} with 4 masked Fourier measurements.

$$\begin{aligned} &= \frac{2}{\sigma_n^2} \sum_{i=1}^M (-2\text{Re}\{\mathbf{A}_i(m, :)\mathbf{x}\} \text{Re}\{\mathbf{A}_i(n, :)\mathbf{x}\} \\ &\quad + (y_i - \mathbf{x}^H \mathbf{A}_i \mathbf{x}) \text{Re}\{[\mathbf{A}_i]_{m,n}\}) \end{aligned} \quad (70)$$

where

$$\frac{\partial \text{Re}\{\mathbf{A}_i(m, :)\mathbf{x}\}}{\partial \text{Re}\{x_n\}} = \text{Re}\{[\mathbf{A}_i]_{m,n}\}. \quad (71)$$

Inserting (70) into (62) yields

$$[\mathbf{F}_{rr}]_{m,n} = \frac{4}{\sigma_n^2} \sum_{i=1}^M \text{Re}\{\mathbf{A}_i(m, :)\mathbf{x}\} \text{Re}\{\mathbf{A}_i(n, :)\mathbf{x}\} \quad (72)$$

which is obtained by using the fact that

$$\mathbb{E}[y_i - \mathbf{x}^H \mathbf{A}_i \mathbf{x}] = 0. \quad (73)$$

The partial derivative of $\ln p(\mathbf{y}; \mathbf{x})$ with respect to the imaginary part of x_m is

$$\frac{\partial \ln p(\mathbf{y}; \mathbf{x})}{\partial \text{Im}\{x_m\}} = \frac{2}{\sigma_n^2} \sum_{i=1}^M (y_i - \mathbf{x}^H \mathbf{A}_i \mathbf{x}) \text{Im}\{\mathbf{A}_i(m, :)\mathbf{x}\} \quad (74)$$

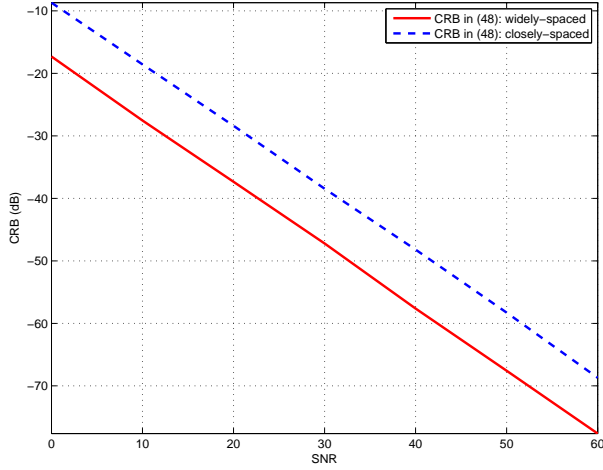


Fig. 10. CRB versus SNR for harmonic retrieval from quadratic measurements.

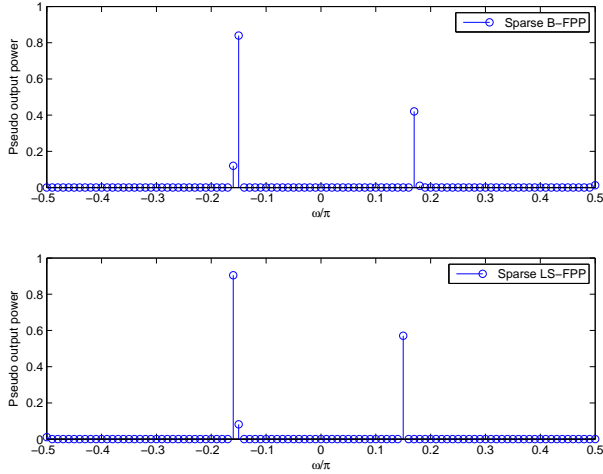


Fig. 11. Signal recovery for harmonic retrieval from quadratic measurements.

where

$$\frac{\partial \mathbf{x}^H \mathbf{A}_i \mathbf{x}}{\partial \text{Im}\{x_m\}} = 2\text{Im}\{\mathbf{A}_i(m, :)\mathbf{x}\}. \quad (75)$$

In a similar manner as we derived (72), it is straightforward to obtain the (m, n) entry of \mathbf{F}_{ii} :

$$[\mathbf{F}_{ii}]_{m,n} = \frac{4}{\sigma_n^2} \sum_{i=1}^M \text{Im}\{\mathbf{A}_i(m, :)\mathbf{x}\} \text{Im}\{\mathbf{A}_i(n, :)\mathbf{x}\}. \quad (76)$$

We now compute the remaining parts of \mathbf{F} . It follows from (69), (74) and (75) that

$$[\mathbf{F}_{ri}]_{m,n} = \frac{4}{\sigma_n^2} \sum_{i=1}^M \text{Re}\{\mathbf{A}_i(m, :)\mathbf{x}\} \text{Im}\{\mathbf{A}_i(n, :)\mathbf{x}\}. \quad (77)$$

Since \mathbf{F} is symmetric, we have

$$\mathbf{F}_{ir} = \mathbf{F}_{ri}^T. \quad (78)$$

By inserting (72), (76), (77) and (78) into (61), we obtain the FIM for phase retrieval of complex-valued \mathbf{x} . Define

$$\mathbf{G}_c = \begin{bmatrix} \text{Re}\{\mathbf{A}_1 \mathbf{x}\} & \cdots & \text{Re}\{\mathbf{A}_M \mathbf{x}\} \\ \text{Im}\{\mathbf{A}_1 \mathbf{x}\} & \cdots & \text{Im}\{\mathbf{A}_M \mathbf{x}\} \end{bmatrix}. \quad (79)$$

\mathbf{F}_c can be further simplified as

$$\mathbf{F}_c = \frac{4}{\sigma_n^2} \mathbf{G}_c \mathbf{G}_c^T. \quad (80)$$

Thus, we complete the proof of Theorem 3.1.

APPENDIX B PROOF OF THEOREM 4.1

The likelihood function for \mathbf{x} = sum-of-harmonics in (40) has the same expression as (58). However, the parameter vector contains the L unknown frequencies and the real and imaginary parts of the L unknown complex amplitudes $\{\gamma_1 \cdots \gamma_L\}$:

$$\boldsymbol{\alpha} = [\omega_1 \cdots \omega_L, \text{Re}\{\gamma_1\} \cdots \text{Re}\{\gamma_L\}, \text{Im}\{\gamma_1\} \cdots \text{Im}\{\gamma_L\}]^T. \quad (81)$$

The FIM associated to $\boldsymbol{\alpha}$ is expressed as

$$\mathbf{F}_v = \begin{bmatrix} \mathbf{F}_{\omega\omega} & \mathbf{F}_{\omega \text{Re}\{\gamma\}} & \mathbf{F}_{\omega \text{Im}\{\gamma\}} \\ \mathbf{F}_{\text{Re}\{\gamma\}\omega} & \mathbf{F}_{\text{Re}\{\gamma\} \text{Re}\{\gamma\}} & \mathbf{F}_{\text{Re}\{\gamma\} \text{Im}\{\gamma\}} \\ \mathbf{F}_{\text{Im}\{\gamma\}\omega} & \mathbf{F}_{\text{Im}\{\gamma\} \text{Re}\{\gamma\}} & \mathbf{F}_{\text{Im}\{\gamma\} \text{Im}\{\gamma\}} \end{bmatrix} \quad (82)$$

where

$$\mathbf{F}_{\text{Re}\{\gamma\}\omega} = \mathbf{F}_{\omega \text{Re}\{\gamma\}}^T \quad (83)$$

$$\mathbf{F}_{\text{Im}\{\gamma\}\omega} = \mathbf{F}_{\omega \text{Im}\{\gamma\}}^T \quad (84)$$

$$\mathbf{F}_{\text{Re}\{\gamma\} \text{Im}\{\gamma\}} = \mathbf{F}_{\text{Im}\{\gamma\} \text{Re}\{\gamma\}}^T. \quad (85)$$

Therefore, we only require to calculate the upper triangular part of \mathbf{F}_v . The first-order derivative of $\ln p(\mathbf{y}; \mathbf{x})$ with respect to $\boldsymbol{\alpha}_m$ is

$$\frac{\partial \ln p(\mathbf{y}; \mathbf{x})}{\partial \boldsymbol{\alpha}_m} = \frac{1}{\sigma_n^2} \sum_{m=1}^M \left((y_i - \mathbf{x}^H \mathbf{A}_i \mathbf{x}) \frac{\partial \mathbf{x}^H \mathbf{A}_i \mathbf{x}}{\partial \boldsymbol{\alpha}_m} \right). \quad (86)$$

Let us first compute

$$\begin{aligned} \frac{\partial \mathbf{x}^H \mathbf{A}_i \mathbf{x}}{\partial \omega_m} &= \gamma_m^* \left(\frac{\partial \mathbf{v}_m}{\partial \omega_m} \right)^H \mathbf{A}_i \mathbf{x} + \gamma_m \mathbf{x}^H \mathbf{A}_i \frac{\partial \mathbf{v}_m}{\partial \omega_m} \\ &= 2\text{Re} \left\{ \gamma_m^* \left(\frac{\partial \mathbf{v}_m}{\partial \omega_m} \right)^H \mathbf{A}_i \mathbf{x} \right\} \end{aligned} \quad (87)$$

where

$$\frac{\partial \mathbf{v}_m}{\partial \omega_m} = [j e^{j\omega_m} \cdots j N e^{jN\omega_m}]^T. \quad (88)$$

In the sequel, we compute

$$\begin{aligned} \frac{\partial^2 \ln p(\mathbf{y}; \mathbf{x})}{\partial \omega_m \partial \omega_n} &= \frac{1}{\sigma_n^2} \sum_{i=1}^M \left((y_i - \mathbf{x}^H \mathbf{A}_i \mathbf{x}) \frac{\partial^2 \mathbf{x}^H \mathbf{A}_i \mathbf{x}}{\partial \omega_m \partial \omega_n} \right. \\ &\quad \left. - \frac{\partial \mathbf{x}^H \mathbf{A}_i \mathbf{x}}{\partial \omega_m} \frac{\partial \mathbf{x}^H \mathbf{A}_i \mathbf{x}}{\partial \omega_n} \right). \end{aligned} \quad (89)$$

To obtain (89), we consider two cases to calculate the value of $\frac{\partial^2 \mathbf{x}^H \mathbf{A}_i \mathbf{x}}{\partial \omega_m \partial \omega_n}$. If $m \neq n$,

$$\frac{\partial^2 \mathbf{x}^H \mathbf{A}_i \mathbf{x}}{\partial \omega_m \partial \omega_n} = 2\text{Re} \left\{ \gamma_m^* \gamma_n \left(\frac{\partial \mathbf{v}_m}{\partial \omega_m} \right)^H \mathbf{A}_i \frac{\partial \mathbf{v}_n}{\partial \omega_n} \right\}. \quad (90)$$

If $m = n$,

$$\begin{aligned} \frac{\partial^2 \mathbf{x}^H \mathbf{A}_i \mathbf{x}}{\partial \omega_m \partial \omega_n} &= 2|\gamma_m|^2 \left(\frac{\partial \mathbf{v}_m}{\partial \omega_m} \right)^H \mathbf{A}_i \frac{\partial \mathbf{v}_m}{\partial \omega_m} \\ &+ 2\text{Re} \left\{ \gamma_m^* \left(\frac{\partial^2 \mathbf{v}_m}{\partial \omega_m^2} \right)^H \mathbf{A}_i \mathbf{x} \right\} \end{aligned} \quad (91)$$

where

$$\frac{\partial^2 \mathbf{v}_m}{\partial \omega_m^2} = - [e^{j\omega_m} \quad \dots \quad N^2 e^{jN\omega_m}]^T. \quad (92)$$

Taking the expectation of both sides of (89) yields

$$\begin{aligned} [\mathbf{F}_{\omega\omega}]_{m,n} &= \frac{4}{\sigma_n^2} \sum_{i=1}^M \text{Re} \left\{ \gamma_m^* \left(\frac{\partial \mathbf{v}_m}{\partial \omega_m} \right)^H \mathbf{A}_i \mathbf{x} \right\} \\ &\times \text{Re} \left\{ \gamma_n^* \left(\frac{\partial \mathbf{v}_n}{\partial \omega_n} \right)^H \mathbf{A}_i \mathbf{x} \right\}. \end{aligned} \quad (93)$$

We next compute $\mathbf{F}_{\omega\text{Re}\{\gamma\}}$. Here, we point out that α_m still corresponds to frequencies while α_n corresponds to the real parts of the amplitudes. The first-order derivative of $\mathbf{x}^H \mathbf{A}_i \mathbf{x}$ w.r.t. $\text{Re}\{\gamma_n\}$ is

$$\frac{\partial \mathbf{x}^H \mathbf{A}_i \mathbf{x}}{\partial \text{Re}\{\gamma_n\}} = \mathbf{v}_n^H \mathbf{A}_i \mathbf{x} + \mathbf{x}^H \mathbf{A}_i \mathbf{v}_n = 2\text{Re}\{\mathbf{v}_n \mathbf{A}_i \mathbf{x}\}. \quad (94)$$

Since the expected value of $(y_i - \mathbf{x}^H \mathbf{A}_i \mathbf{x})$ is zero, we directly obtain

$$\begin{aligned} [\mathbf{F}_{\omega\text{Re}\{\gamma\}}]_{m,n} &= \frac{4}{\sigma_n^2} \sum_{i=1}^M \text{Re} \left\{ \gamma_m^* \left(\frac{\partial \mathbf{v}_m}{\partial \omega_m} \right)^H \mathbf{A}_i \mathbf{x} \right\} \\ &\times \text{Re} \left\{ \mathbf{v}_n^H \mathbf{A}_i \mathbf{x} \right\}. \end{aligned} \quad (95)$$

In a similar manner as we calculated $\frac{\partial \mathbf{x}^H \mathbf{A}_i \mathbf{x}}{\partial \text{Re}\{\gamma_n\}}$, the first-order derivative of $\mathbf{x}^H \mathbf{A}_i \mathbf{x}$ w.r.t. $\text{Im}\{\gamma_n\}$ is

$$\frac{\partial \mathbf{x}^H \mathbf{A}_i \mathbf{x}}{\partial \text{Im}\{\gamma_n\}} = 2\text{Im}\{\mathbf{v}_n \mathbf{A}_i \mathbf{x}\} \quad (96)$$

which results in the following formula for $\mathbf{F}_{\omega\text{Im}\{\gamma\}}$

$$\begin{aligned} [\mathbf{F}_{\omega\text{Im}\{\gamma\}}]_{m,n} &= \frac{4}{\sigma_n^2} \sum_{i=1}^M \text{Re} \left\{ \gamma_m^* \left(\frac{\partial \mathbf{v}_m}{\partial \omega_m} \right)^H \mathbf{A}_i \mathbf{x} \right\} \\ &\times \text{Im} \left\{ \mathbf{v}_n^H \mathbf{A}_i \mathbf{x} \right\}. \end{aligned} \quad (97)$$

At this point, the expressions for $\mathbf{F}_{\text{Re}\{\gamma\}\text{Re}\{\gamma\}}$ and $\mathbf{F}_{\text{Im}\{\gamma\}\text{Im}\{\gamma\}}$ can be easily derived

$$\mathbf{F}_{\text{Re}\{\gamma\}\text{Re}\{\gamma\}} = \frac{4}{\sigma_n^2} \sum_{i=1}^M \text{Re} \left\{ \mathbf{v}_m^H \mathbf{A}_i \mathbf{x} \right\} \text{Re} \left\{ \mathbf{v}_n^H \mathbf{A}_i \mathbf{x} \right\} \quad (98)$$

$$\mathbf{F}_{\text{Im}\{\gamma\}\text{Im}\{\gamma\}} = \frac{4}{\sigma_n^2} \sum_{i=1}^M \text{Im} \left\{ \mathbf{v}_m^H \mathbf{A}_i \mathbf{x} \right\} \text{Im} \left\{ \mathbf{v}_n^H \mathbf{A}_i \mathbf{x} \right\}. \quad (99)$$

Substituting (93), (95), (97), (98) and (99) into (82), after some matrix manipulations, we have

$$\mathbf{F}_v = \frac{4}{\sigma_n^2} \mathbf{G}_v \mathbf{G}_v^T \quad (100)$$

where

$$\mathbf{G}_v = \begin{bmatrix} \text{Re}\{\mathbf{X}^H \mathbf{A}_1 \mathbf{x}\} & \dots & \text{Re}\{\mathbf{X}^H \mathbf{A}_M \mathbf{x}\} \\ \text{Re}\{\mathbf{V}^H \mathbf{A}_1 \mathbf{x}\} & \dots & \text{Re}\{\mathbf{V}^H \mathbf{A}_M \mathbf{x}\} \\ \text{Im}\{\mathbf{V}^H \mathbf{A}_1 \mathbf{x}\} & \dots & \text{Im}\{\mathbf{V}^H \mathbf{A}_M \mathbf{x}\} \end{bmatrix} \quad (101)$$

$$\mathbf{X} = \begin{bmatrix} \gamma_1 \frac{\partial \mathbf{v}_1}{\partial \omega_1} & \dots & \gamma_L \frac{\partial \mathbf{v}_L}{\partial \omega_L} \end{bmatrix} \quad (102)$$

$$\mathbf{V} = [\mathbf{v}(\omega_1) \quad \dots \quad \mathbf{v}(\omega_L)]. \quad (103)$$

Note that similar to the FIM of the CRB for complex-valued \mathbf{x} , i.e., (22), \mathbf{F}_v is also rank-1 deficient. Thus, the CRB for sum-of-harmonics \mathbf{x} is computed by using the pseudo-inverse of \mathbf{F}_v . Thus, we have proved Theorem 4.1.

REFERENCES

- [1] R. W. Harrison, "Phase problem in crystallography," *Journal of the Optical Society of America A*, vol. 10, no. 5, pp. 1046-1055, 1993.
- [2] O. Bunk, A. Diaz, F. Pfeiffer, C. David, B. Schmitt, D. K. Satpathy and J. F. van der Veen, "Diffractive imaging for periodic samples: Retrieving one-dimensional concentration profiles across microfluidic channels," *Acta Crystallographica Section A: Foundations of Crystallography*, vol. 63, no. 4, pp. 306-314, 2007.
- [3] F. Pfeiffer, T. Weitkamp, O. Bunk and C. David, "Phase retrieval and differential phase-contrast imaging with low-brilliance X-ray sources," *Nature Physics*, vol. 2, no. 4, pp. 258-261, 2006.
- [4] J. Miao, T. Ishikawa, Q. Shen and T, "Extending X-ray crystallography to allow the imaging of noncrystalline materials, cells, and single protein complexes," *Annu. Rev. Phys. Chem.*, vol. 59, pp. 387-410, 2008.
- [5] F. Hüe, J. M. Rodenburg, A. M. Maiden, F. Sweeney and P. A. Midgley, "Wave-front phase retrieval in transmission electron microscopy via ptychography," *Physical Review B*, vol. 82, no. 12, pp. 121415, 2010.
- [6] R. Gerchberg and W. Saxton, "A practical algorithm for the determination of phase from image and diffraction plane pictures," *Optik*, vol. 35, pp. 237-246, 1972.
- [7] J. R. Fienup, "Phase retrieval algorithms: A comparison," *Applied Optics*, vol. 21, no. 15, pp. 2758-2769, 1982.
- [8] E. J. Candès, T. Strohmer, and V. Voroninski. "PhaseLift: Exact and stable signal recovery from magnitude measurements via convex programming," *Communications on Pure and Applied Mathematics*, vol. 66, no. 8, pp. 1241-1274, 2013.
- [9] E. J. Candès, Y. C. Eldar, T. Strohmer and V. Voroninski, "Phase retrieval via matrix completion," *SIAM Review*, vol. 57, no. 2 pp. 225-251, 2015.
- [10] Z. Luo, W. Ma, A. M. C. So, Y. Ye and S. Zhang, "Semidefinite relaxation of quadratic optimization problems," *IEEE Signal Process. Magazine*, vol. 27, no. 3, pp. 20-34, 2010.
- [11] Y. Shechtman, Y. C. Eldar, O. Cohen, H. N. Chapman, J. Miao and M. Segev, "Phase retrieval with application to optical imaging: A contemporary overview," *IEEE Signal Process. Magazine*, vol. 32, no. 3, pp. 87-109, 2015.
- [12] I. Waldspurger, A. d'Aspremont, and S. Mallat, "Phase recovery, maxcut and complex semidefinite programming," *Mathematical Programming*, vol. 149, no. 1-2, pp. 47-81, 2015.
- [13] E. J. Candès, X. Li and M. Soltanolkotabi, "Phase retrieval via Wirtinger Flow: Theory and algorithms," *IEEE Trans. Information Theory*, vol. 61, no. 4, pp. 1985-2007, 2015.
- [14] O. Mehanha, K. Huang, B. Gopalakrishnan, A. Konar and N. S. Sidiropoulos, "Feasible point pursuit and successive approximation of non-convex QCQPs," *IEEE Signal Process. Letters*, vol. 22, no. 7, pp. 804-808, 2015.
- [15] R. Balan, "Reconstruction of signals from magnitudes of redundant representations," *arXiv preprint arXiv*, 1207.1134, 2012.
- [16] R. Balan, "Reconstruction of signals from magnitudes of redundant representations: The complex case," *Foundations of Computational Mathematics*, pp. 1-45, 2013.
- [17] R. Balan, "The Fisher information matrix and the CRLB in a non-AWGN model for the phase retrieval problem," *Proc. of 2015 Internat. Conf. on Sampl. Theory and Applications (SampTA)*, pp. 178-182, Washington, DC, 2015.
- [18] J. N. Cederquist and C. C. Wackerman, "Phase-retrieval error: A lower bound," *Journal of the Optical Society of America A*, vol. 4, no. 9, pp. 1788-1792, 1987.

- [19] H. Sahinoglou and S. Cabrera, "On phase retrieval of finite-length sequences using the initial time sample," *IEEE Trans. Circuits and Systems*, vol. 38, no. 5, pp. 954-958, 1991.
- [20] C. Helmberg, F. Rendl, R. J. Vanderbei and H. Wolkowicz, "An interior-point method for semidefinite programming," *SIAM Journal on Optimization*, vol. 6, no. 2, pp. 342-361, 1996.
- [21] S. J. Kim, K. Koh, M. Lustig, S. Boyd and D. Gorinevsky, "An interior-point method for large-scale ℓ_1 -regularized least squares," *IEEE Journal of Selected Topics in Signal Process.*, vol. 1, no. 4, pp. 606-617, 2007.
- [22] S. Basu and Y. Bresler, "The stability of nonlinear least squares problems and the Cramér-Rao bound," *IEEE Trans. Signal Process.*, vol. 48, no. 12, pp. 3426-3436, 2000.
- [23] A. Swami, "Cramér-Rao bounds for deterministic signals in additive and multiplicative noise," *Signal Process.*, vol. 53, no. 23, pp. 2312-2324, 1996.
- [24] P. Stoica and T. L. Marzetta, "Parameter estimation problems with singular information matrices," *IEEE Trans. Signal Process.*, vol. 49, no. 1, pp. 87-90, 2001.
- [25] A. O. Hero, III, J. A. Fessler and M. Usman, "Exploring estimator bias-variance tradeoffs using the uniform CR bound," *IEEE Trans. Signal Process.*, vol. 44, pp. 2026-2041, 1996.
- [26] C. R. Rao, *Linear statistical inference and its applications*, 2nd ed. New York: Wiley, 1973.
- [27] K. Huang and N. D. Sidiropoulos, "Putting nonnegative matrix factorization to the test: A tutorial derivation of pertinent Cramér-Rao bounds and performance benchmarking," *IEEE Signal Processing Magazine, Special Issue on Source Separation and Applications*, vol. 31, no. 3, pp. 76-86, 2014.
- [28] G. Golub and K. William, "Calculating the singular values and pseudo-inverse of a matrix," *Journal of the Society for Industrial & Applied Mathematics, Series B: Numerical Analysis*, vol. 2, no. 2, pp. 205-224, 1965.
- [29] K. Heonhwan, A. M. Haimovich and Y. C. Eldar, "Non-coherent direction of arrival estimation from magnitude-only measurements," *IEEE Signal Process. Letters*, vol. 22, no. 7, pp. 925-929, 2015.
- [30] S. S. Chen, D. L. Donoho and M. A. Saunders, "Atomic decomposition by basis pursuit," *SIAM J. Scientific Computing*, vol. 20, no. 1, pp. 33-61, 1998.
- [31] D. L. Donoho and X. Huo, "Uncertainty principles and ideal atomic decomposition," *IEEE Trans. Information Theory*, vol. 47, no. 7, pp. 2845-2862, 2001.